Thin Solid Films 517 (2009) 5813–5818

Contents lists available at ScienceDirect

Thin Solid Films

journal homepage: www.elsevier.com/locate/tsf

Synthesis and photoelectrochemical properties of thin bismuth molybdates film with various crystal phases

Xu Zhao [a,b,*], Tongguang Xu [a], Wenqing Yao [a], Yongfa Zhu [a,*]

[a] Department of Chemistry, Tsinghua University, Beijing, 100084, PR China
[b] State Key Laboratory of Environmental Aquatic Chemistry, Research Center for Eco-Environmental Science, Chinese Academy of Sciences, Beijing, 100085, PR China

ARTICLE INFO

Article history:
Received 23 July 2008
Received in revised form 23 February 2009
Accepted 27 February 2009
Available online 9 March 2009

Keywords:
Bismuth molybdate film
Photoelectrochemical properties
Visible light
Crystal structure
X-ray diffraction
Optical spectroscopy
Chemical solution deposition

ABSTRACT

Bismuth molybdate films with various phase structures including α-$Bi_2Mo_3O_{12}$, β-$Bi_2Mo_2O_9$, γ-Bi_2MoO_6, and γ′-Bi_2MoO_6 are fabricated on the indium–tin oxide glass substrates from an amorphous heteronuclear complex via the dip-coating method by appropriate adjustment of the reaction conditions. α-$Bi_2Mo_3O_{12}$, β-$Bi_2Mo_2O_9$, and γ-Bi_2MoO_6 film can be obtained at 400 °C, 500 °C, and 500 °C for 1 h, respectively. At 500 °C, γ′-Bi_2MoO_6 can be obtained for 4 h. Film formation process is proposed based on the experimental results. Thin γ-Bi_2MoO_6 films exhibit high photoresponse under visible light irradiation. Incident photon to current conversion efficiency of thin γ-Bi_2MoO_6 film starts to increase near 450 nm. And, it can reach 4.1% at 400 nm. The top of the valence band and bottom of the conduction band are roughly estimated to be −0.71 and 1.69 eV, respectively. In contrast, γ′-Bi_2MoO_6 generated weak photocurrent; α-$Bi_2Mo_3O_{12}$ and β-$Bi_2Mo_2O_9$ film has no photoresponse under visible light irradiation. The reason for the difference in the visible light response was discussed.

1. Introduction

Photocatalysts that respond to visible light are needed to utilize the main part of the solar spectrum for the production of hydrogen energy by splitting water [1], solar energy cell [2], and other applications [3]. Traditional visible-light photocatalysts are either unstable upon illumination with light or have low activity [4]. Recently, some UV-active oxides functioned as visible-light photocatalysts by doping of metal [5], N, C, and S [6]. However, these doped materials, in general, show a small absorption in the visible-light region, leading to low activities [7]. Thus, it is very important to develop more efficient visible-light photocatalysts.

Bismuth molybdates have the general chemical formula of Bi_2O_3 $nMoO_3$ where $n=3$, 2, or 1, corresponding to α, β, γ, and γ′ phase, respectively. Such compounds and their mixtures are well known due to their catalytic application in the area of selective oxidation/oxidative dehydrogenation or ammoxidation of lower olefins [8]. However, each phase exhibits different properties. Recently, photocatalytic activities of Bi_2WO_6 have been revealed by Kudo and Hijii [9], Tang et al. [10], and our group [11]. These works revealed tungstates could be performed as good photocatalytic materials under visible light irradiation. Usually, the molybdates have the same crystalline pattern as the tungstates, implying they can also be used as photocatalyst. Kudo and his collaborators found that Bi_2MoO_6 was able to the photocatalytic O_2-evolution under visible light irradiation [9,12]. However, its photoelectrochemical (PEC) properties and effect of crystal phases on its PEC properties are still unknown now. Herein, bismuth molybdates films with various crystal phases were fabricated from amorphous heteronuclear complex via dip-coating method. γ-Bi_2MoO_6 film exhibited high photocurrent response under visible light irradiation. In contrast, γ′-Bi_2MoO_6 films generated weak photocurrent; α-$Bi_2Mo_3O_{12}$ and β-$Bi_2Mo_2O_9$ film nearly had no photoresponse. And, their photoelectrochemical properties were discussed and electron structure of γ-Bi_2MoO_6 was explored.

2. Experimental section

2.1. Fabrication of bismuth molybdate films

Indium–tin oxide (ITO) glass was purchased from China Southern Class Co. Ltd., with a thickness of 1.1 mm and a sheet resistance of 15 Ω/square. The thickness of the ITO layer was 1×10^{-4} mm. All other chemicals are analytical grade reagents and used without further purification. Deionized water was used throughout the experiment. Fabrication of bismuth molybdate films includes preparation of precursor and subsequent deposition and calcinations. Procedures were described below in details. 4.85 g $Bi(NO_3)_3$ $5H_2O$ was dissolved in 30 ml water. Following, 10 ml strong ammonia water (28% by weight) was added slowly and the pH of the solution was ca. 7. After the precipitates were dispersed completely by

* Corresponding author. Tel.: +86 10 62787601.
E-mail addresses: enzx76@yahoo.com.cn (X. Zhao), zhuyf@mail.tsinghua.edu.cn (Y. Zhu).

0040-6090/$ – see front matter © 2009 Published by Elsevier B.V.
doi:10.1016/j.tsf.2009.02.135

ultrasonic method, 0.72 g MoO_3 was added. The above suspension was stirred and heated to be 80 °C. Then, 9.83 g diethylenetriaminepent acetic acid was added. The obtained suspension was stirred and heated at ca. 80 °C until the mixture became a transparent solution. After being vaporized slowly at 80 °C, a piece of transparent glass-like material was obtained, which was named as precursor. The precursor dissolved in aqueous solution (20%, by weight) was deposited onto an ITO glass via dip-coating method, and calcined at various temperatures in air for various time.

2.2. Characterization of bismuth molybdate films

Morphology of the bismuth molybdates films was characterized by a JSM 6301 electron-scanning microscope (SEM). Raman spectra were conducted on a Renishaw RM1000 spectroscope. The wavelength of the laser light was 514 nm. X-ray diffraction (XRD) was performed on the X-Ray Diffractometer (Japan, Rigaku, D/max-RB) for monochromatizaed Cu Kα (λ = 1.5418 Å) radiation. Thermogravimetry-differential thermal analysis (TG-DTA) was performed on a Du Pont Universal V2.6D thermal analyzer. The atmosphere is air and the heating rate is 10 °C/min. Fourier transform infrared spectroscopy (FT-IR, Spectrum GX, Perkin-Elmer Company) was used for the assessment of the crystallization of the precursor films. The Auger electron spectroscopy technique was used to determine the thickness of the film. The energy and beam current of the Ar ion beam were 3.0 keV and 6 μA, respectively. The beam diameter was 1 mm and the sputtering rate was approximately 30.0 nm/min. The film thickness can be determined to be 450 nm.

2.3. Photoelectrochemical properties of bismuth molybdate films

The photoelectrochemical experiment was carried out using a PARSTAT 2273 advanced electrochemical system (Princeton Applied Research) with a Lock-In amplifier (Model SR830 DSP, Stanford research systems). For photoelectrochemical measurement, a Cu wire was attached to the bismuth molybdate film with epoxy resin to prevent current leakage. A quartz electrolytic cell was employed, filled with 20 mL of 0.1 M KCl solution. A Pt wire and a saturated calomel electrode (SCE) were employed as the counter and reference electrodes, respectively. A 300 W Xe lamp was used as irradiation source.

3. Results and discussion

3.1. Structure and texture of bismuth molybdates films

Fig. 1(A) shows the Raman patterns for the precursor film treated at various temperatures for 1 h. The precursor film was amorphous.

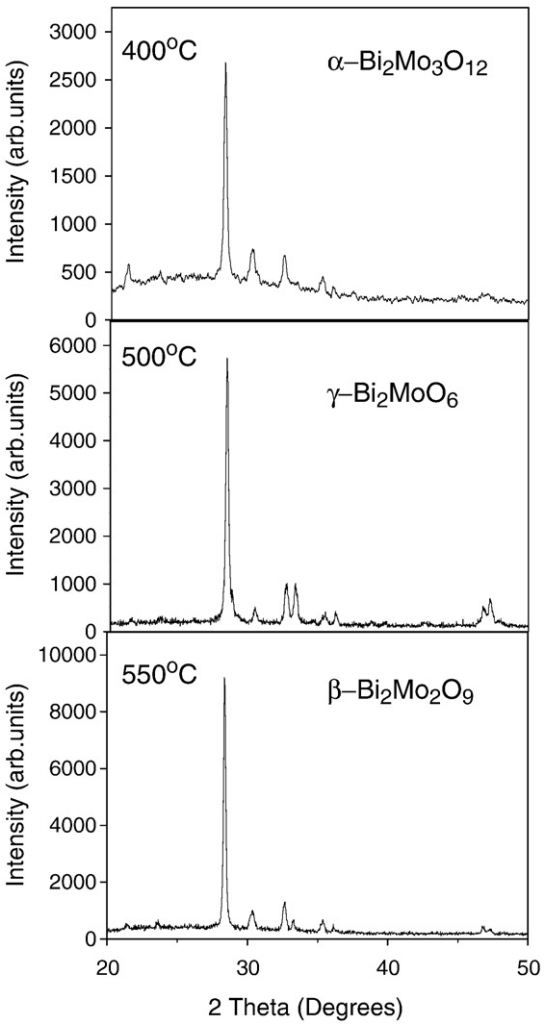

Fig. 2. X-ray diffraction analysis of the precursor film treated at various temperatures for 1 h.

And, the crystalline phase of α-$Bi_2Mo_3O_{12}$ with the specific band at 899 cm^{-1} appears at the treated temperature of 400 °C; the crystalline phase of γ-Bi_2MoO_6 with the specific band at 804 cm^{-1} appear at 500 °C; the β-$Bi_2Mo_2O_9$ with the specific band at 884 cm^{-1} appears when the temperature is increased to 550 °C. The effect of calcination time on the crystallization of bismuth molybdates were

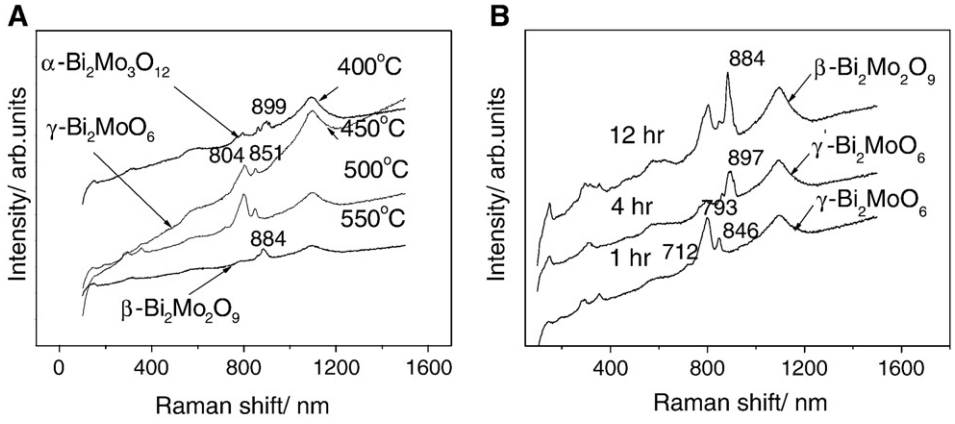

Fig. 1. Raman spectroscopy of the precursor film treated at various conditions. A, different temperatures for 1 h; B, different time at 500 °C.

investigated at the temperature of 500 °C. For the film sample calcined for 1 h, the strong antisymmetric stretching Mo–O mode observed at 793 cm^{-1} for the distorted MoO_6 octahedra indicate the formation of the γ-Bi_2MoO_6 phase. In contrast, the Raman spectrum of the film samples treated for 4 h show a strong antisymmetric stretching Mo–O mode at 890 cm^{-1}, which is characteristic of MoO_4 tetrahedra [8]. The above result indicates the formation of γ'-Bi_2MoO_6 phase. When the calcination time is extended to 12 h, β-$Bi_2Mo_2O_9$ appears. Furthermore, the film samples treated at 400 °C, 500 °C, and 550 °C for 1 h were analyzed by XRD method. As shown in Fig. 2, the film samples treated at 400 °C, 500 °C, and 550 °C can be identified as α-$Bi_2Mo_3O_{12}$ (JCPDS 21-103), γ-Bi_2MoO_6 (JCPDS 21-102), and β-$Bi_2Mo_2O_9$ (JCPDS 33-209), respectively (Joint Committee on Powder Diffraction Standards, ASTM).

The precursor film was obtained by drying the precursor solution with the initial concentration of 20% at 90 °C. As shown in Fig. 3, it was uniform and its morphologies change with the annealing temperature. The sample heated at 400 °C for 1 h consists of a network of ca. 120 nm round particles with the crystalline phase of α-$Bi_2Mo_3O_{12}$. Annealing of a precursor sample at 500 °C for 1 h leads to the formation of the γ-Bi_2MoO_6 film, which is homogeneous and composed of about 70 nm sized, regular particles and exhibits substantial porosity. At the temperature of 500 °C for 4 h, the γ'-Bi_2MoO_6 phase appear with large particle size; for 12 h, the β-$Bi_2Mo_2O_9$ with the rod-like particles is observed.

In order to explore the formation process of the bismuth molybdate film, the decomposition process of the precursor powders was investigated using TG and DTA curves. As shown in Fig. 4, with the increase of temperature, the weight loss occurs in the TG curve up to 500 °C. Thereafter, the weight remains constant, indicating that the decomposition of all organic materials continued in the precursor; their combustion and crystallization of bismuth molybdates have been completed below 500 °C. No significant plateau, corresponding to well-defined intermediate products, appeared in the heating process.

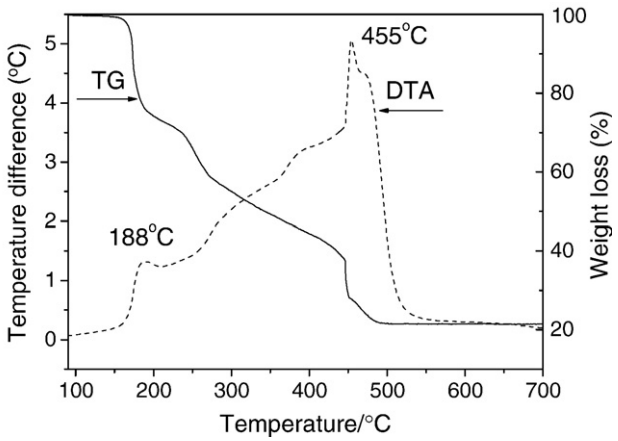

Fig. 4. TG-DTA analysis of the precursor samples.

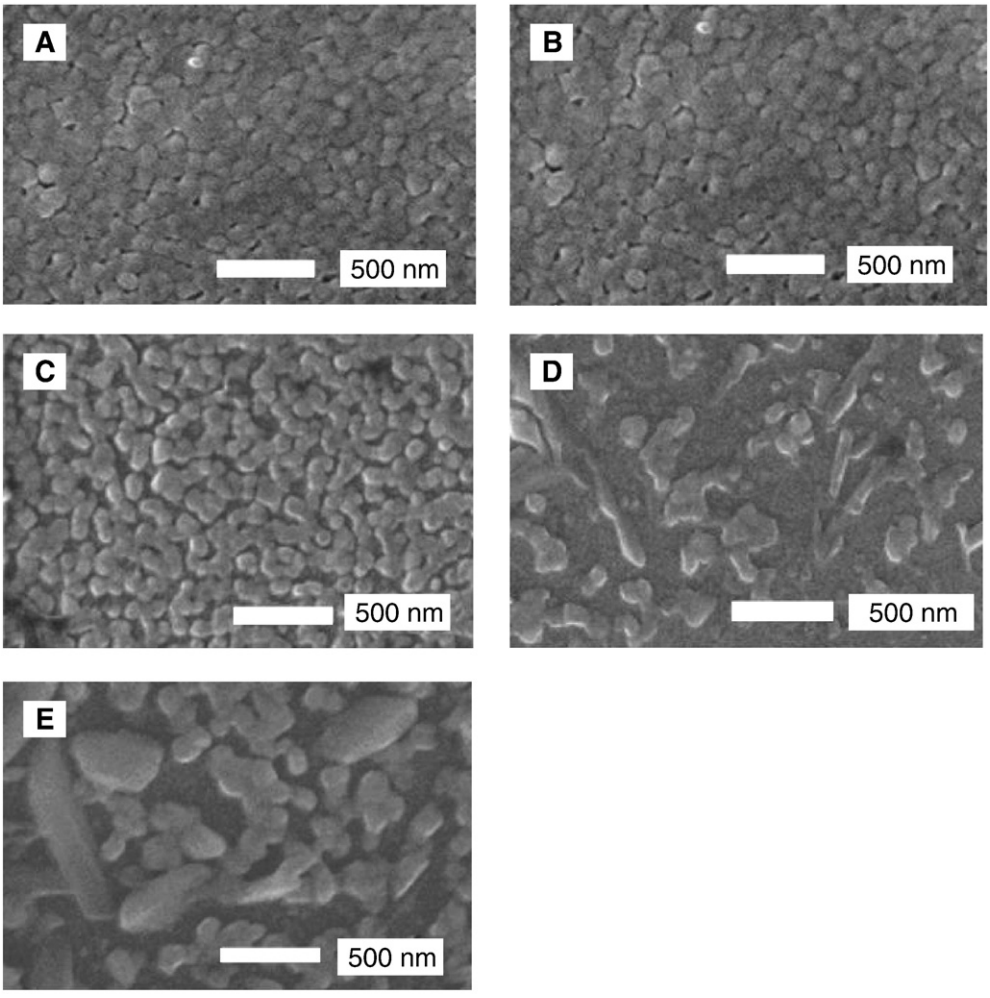

Fig. 3. SEM of the precursor film treated at various conditions (A, Precursor; B, 400 °C for 1 h; C, 500 °C for 1 h; D, 500 °C for 4 h; E, 500 °C for 12 h).

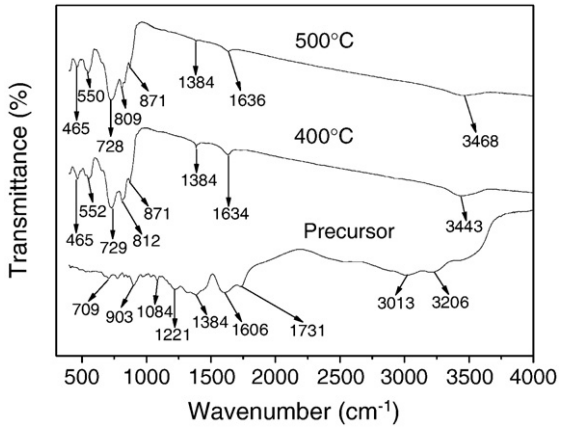

Fig. 5. FT-IR spectra of precursor samples recorded at various temperatures in air.

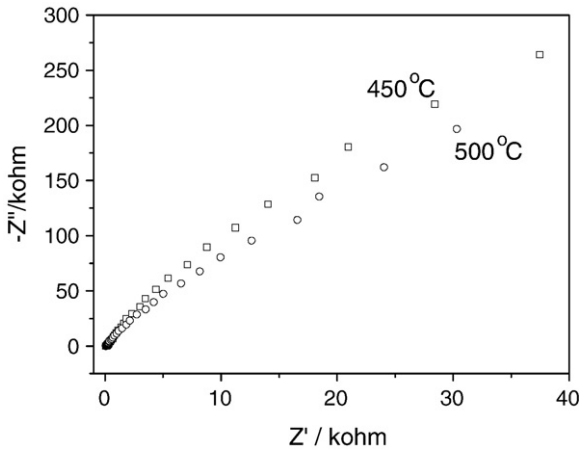

Fig. 7. Electrochemical impedance spectra plane display of the γ-Bi_2MoO_6 film samples treated at 450 °C and 500 °C.

DTA curve shows two exothermic peaks which could be further classified into two types of physical meaning: (1) left exothermic peaks at 188 °C correspond to initial decomposition of the precursor and (2) right exothermic peaks at 455 °C correspond to the formation of the nucleus of the crystal and crystallization of γ-Bi_2MoO_6. Below 455 °C, the resulting powders were dark brown, hard and porous, denoting an amorphous phase. It is attributed to contain a lot of carbons and ignitable organics. At the temperature of 455 °C, crystal nuclear begins to form, and the primary crystallizing process has been completed accompanying the combustion of the residual carbons and ignitable organics.

Furthermore, the precursor powder sample and precursor samples treated at 450 and 500 °C for 1 h were analyzed by FT-IR. The results are presented in Fig. 5. The bands of FT-IR spectra of the precursor film at 3206, 3013, 1731, 1606, 1221, 1084, 903, and 709 cm^{-1} originated from the NH_2, C–N, C=O, C–O, and C–H bands. Above 400 °C, these bands almost completely disappear. For the sample treated at 400 °C, the bands of 729, 812, and 871 cm^{-1} are assigned to Mo–O stretching bands; the bands of 465 and 552 cm^{-1} are assigned to the stretching and deformation modes involving Bi–O modes. These bands can be ascribed to vibration modes of bismuth molybdates according to data in the literature [13]. No noticeable change is observed in the samples treated at 400 °C and 500 °C. In deed, IR spectra reported in the literature for α, β, and γ phase display strong absorptions in the same frequency range [14].

3.2. Photoelectrochemical properties of the bismuth molybdates films

Fig. 6 shows the current–voltage plots for the precursor film annealed at various temperatures under the condition of dark or visible light irradiation, respectively. There was a significant photocurrent generation for the film samples treated at 450 and 500 °C for 1 h (Fig. 6(A)). However, no photocurrent generation is observed for the film samples treated at 400 and 550 °C. From Fig. 6(B), it can be seen that the photocurrent density for the film samples treated at 500 °C for 1 h was larger than that of the film samples treated for 4 h. Moreover, the photocurrent is nearly not observed for the film samples treated for 12 h.

It is clear that the γ phase for the Bi_2MoO_6 film has higher photocurrent response than the γ' phase for the Bi_2MoO_6 film under visible light irradiation. No photocurrent is generated from the α-$Bi_2Mo_3O_{12}$ and β-$Bi_2Mo_2O_9$ film. γ-Bi_2MoO_6 consists of Mo–O, O, and Bi–O layers. Mo and oxygen exists as distorted octahedral structure. γ'-Bi_2MoO_6 has twin Mo tetrahedral structure and Mo and Bi ions lies on the same plane [15]. This difference probably affects the charge separation and delocalization of photogenerated electrons and holes. The α- and β-phases differ substantially in structure from the γ-phase. The structures of the α- and β-phases can be considered as defective fluorite structures, whereas the γ-phase is an Aurivillius-type structure [16]. Shimodaira et al. [17] revealed that only these materials containing MoO_6 octahedra in the structure showed the photocatalytic activity whereas those containing MoO_4 tetrahedra showed negligible photocatalytic activities among the bismuth molybdates. Our results are consistent with it. It is considered that Bi_2MoO_6 showed higher activity than $Bi_2Mo_3O_{12}$ is the crystal structure. Bi_2MoO_6 possessed perovskite-like slabs consisting of MoO_6 octahedra of which the structure is often advantageous for photocatalysts because excitation energy can easily migrate in the

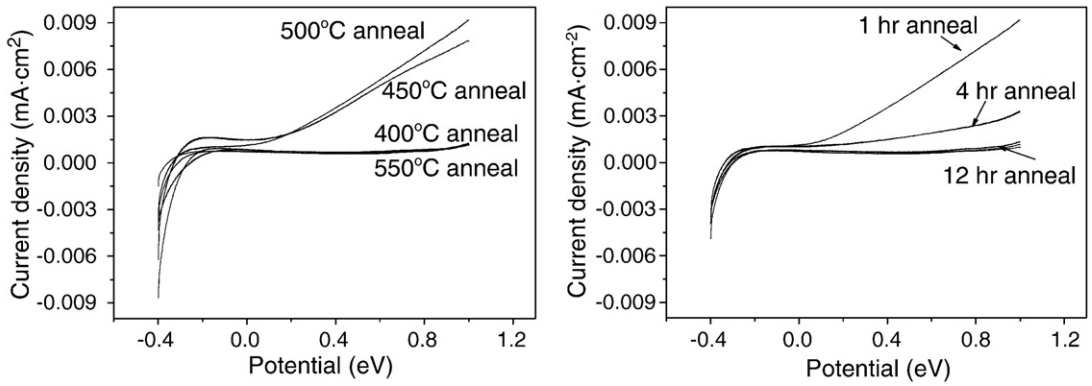

Fig. 6. Photocurrent response for the film samples treated at various conditions versus the applied bias potentials under visible light irradiation (λ>420 nm) with light intensity of 150 mW/cm^2. A, different temperatures for 1 h; B, different time at 500 °C.

structure. With respect to the γ-Bi_2MoO_6 film samples, higher photocurrent for the film sample treated at 500 °C than that treated at 450 °C can be due to the relatively large size of the particles and the nature of the interparticle contacts. In such a situation, the electrical contact at the interface can be improved. As a result of the improved electrical contact at the γ-Bi_2MoO_6 interface and the blocking of the γ-Bi_2MoO_6 surface states, the overall charge-transfer resistance of the film treated at 500 °C appears to be smaller compared with that of the film samples treated at 450 °C, as shown in Fig. 7.

Incident photon to current conversion efficiency (IPCE) defined as the number of electrons collected per incident photon, was evaluated from short circuit photocurrent (I_{sc}) measurements at different wavelengths (λ) and using the following expression (Eq. (1)):

$$\mathrm{IPCE\%} = \left[1240 \times I_{sc}\left(\mathrm{mA/cm^2}\right)\right] / \left[\lambda(\mathrm{nm}) \times I_{inc}\left(\mathrm{mW/cm^2}\right)\right] \times 100 \quad (1)$$

Where I_{inc} is the incident light intensity. As shown in Fig. 8, the IPCE value of γ-Bi_2MoO_6 film is higher than that of the γ′-Bi_2MoO_6 film. In contrast, no IPCE response is observed for the α-$Bi_2Mo_3O_{12}$ and β-$Bi_2Mo_2O_9$ film. For the γ-Bi_2MoO_6 film, IPCE starts to increase near 450 nm. It can reach 4.1% at 400 nm. The above results are consistent with the photocurrent response as shown in Fig. 6.

Fig. 9(A) showed a typical diffuse reflection spectrum of γ-Bi_2MoO_6 powder treated at 500 °C for 1 h. The steep shape of the spectra indicated that the visible light absorption was not due to the transition from the impurity level but was due to the band-gap transition [18]. The band gap energy, E_g of the γ-Bi_2MoO_6 powder is determined using the following equation [19], $ahv = A(hv - E_g)^{1/2}$, where a, v, E_g, and A are absorption coefficient, light frequency, band gap, and a constant, respectively. The band gap energy of the γ-Bi_2MoO_6 film was estimated to be 2.40 eV. For the γ-Bi_2MoO_6 phase, the band starts at 480 nm, which is originated by the $O^{2-} \rightarrow Mo^{6+}$ charge transfer process for octahedral [MoO_6] species. In contrast, the corresponding band for [MoO_4] species existing in α-$Bi_2Mo_3O_{12}$, is expected at 440 nm; And, the β-$Bi_2Mo_3O_{12}$ has two absorption bands at 526 (very weak) and 580 nm, together with the beginning of a charge transfer band at 480 nm; this band can be ascribed to [MoO_6] species, while the bands at 526 and 580 nm can be ascribed to octahedral [MoO_6] species [20]. It is well known that the flatband potential (E_{fb}) of a semiconductor can be obtained from the intercept of Mott–Schottky plot [21]. Fig. 9(B) shows the Mott–Schottky plot for the γ-Bi_2MoO_6 film in the electrolyte solution of 0.1 M KCl in the dark. Straight line is observed; a single intercept is obtained at −0.51 V/SCE, giving a flatband potential of 0.51 V/SCE approximately.

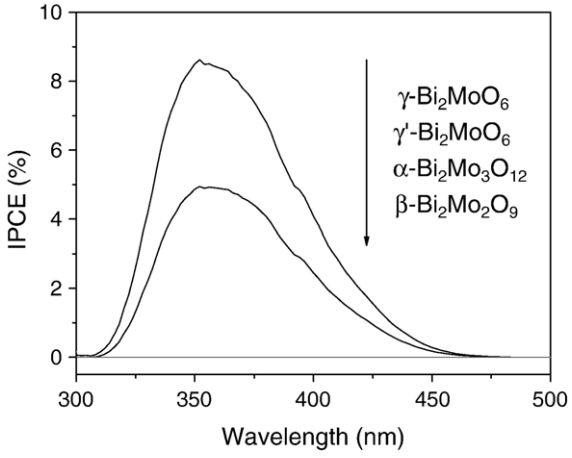

Fig. 8. IPCE vs. λ for the α-$Bi_2Mo_3O_{12}$, β-$Bi_2Mo_2O_9$, γ-Bi_2MoO_6, and γ′-Bi_2MoO_6 film electrode in 0.1 M KCl solution at various potentials under monochromatic light irradiation.

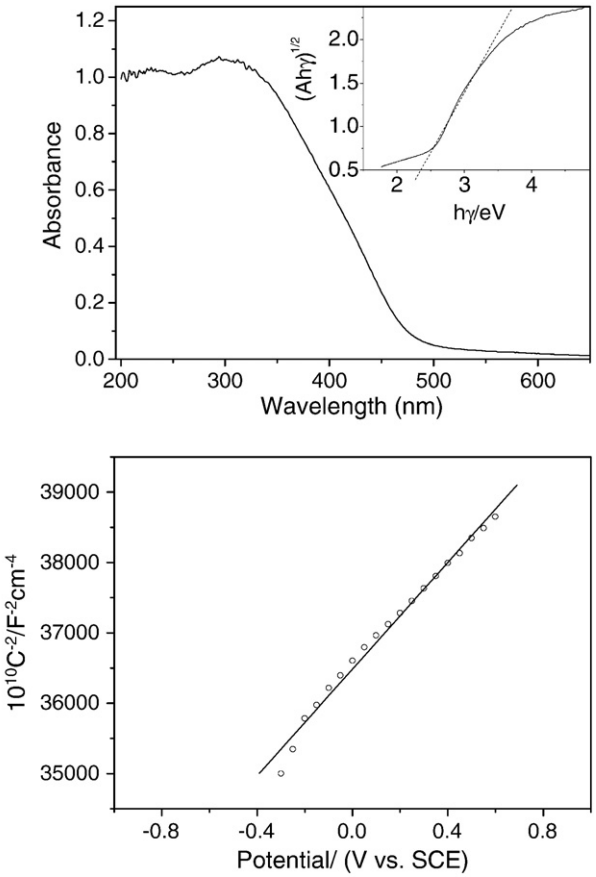

Fig. 9. UV–Vis diffuse reflectance spectroscopy of the γ-Bi_2MoO_6 powder and Mott–Schottky plot of the γ-Bi_2MoO_6 film in 0.1 M KCl solution (the frequency of the ac signal was 1 kHz).

4. Conclusion

Thin bismuth molybdate films with various crystal phase structures can be fabricated from an amorphous heteronuclear complex via the dip-coating method by the adjustment of reaction time and temperature. Under visible light irradiation, the photocurrent generated from γ-Bi_2MoO_6 is higher than that of γ′-Bi_2MoO_6. Distortion of Bi–O band was suggested to contribute to the different photocurrent response. No photocurrent was generated from α-$Bi_2Mo_3O_{12}$ and β-$Bi_2Mo_2O_9$ film. For the γ-Bi_2MoO_6 film, IPCE of 4.1% can be obtained at 400 nm. Many parts of the fabrication including variation of surface texture and film thickness have still to be optimized and we expect that the efficiency of the γ-Bi_2MoO_6 film can be improved.

Acknowledgement

This work was supported by Chinese National Science Foundation (20837001, 20673065, 50778172).

References

[1] A. Fujishima, K. Honda, Nature 238 (1972) 37.
[2] M. Gratzel, Nature 414 (2001) 338.
[3] M.R. Hoffman, S.T. Martin, W. Choi, D.W. Bahnemann, Chem. Rev. 95 (1995) 69.
[4] D.W. Hwang, J. Kim, T.J. Park, J.S. Lee, Catal. Lett. 80 (2002) 53.
[5] Z.G. Zou, J.H. Ye, K. Sayama, H. Arakawa, Nature 414 (2001) 625.
[6] A. Ishikawa, T. Takata, J.N. Kondo, M. Hara, H. Kobayashi, K. Domen, J. Am. Chem. Soc. 124 (2002) 547.
[7] D.W. Hwang, H.G. Kim, J.S. Lee, J. Kim, W. Li, S.H. Oh, J. Phys. Chem. B. 109 (2005) 2093.

[8] A.M. Beale, G. Sankar, Chem. Mater. 15 (2003) 146.
[9] A. Kudo, S. Hijii, Chem. Lett. (1999) 1103.
[10] J.W. Tang, Z.G. Zou, J.H. Ye, Catal. Lett. 92 (2004) 53.
[11] C. Zhang, Y.F. Zhu, Chem. Mater. 17 (2005) 3537.
[12] J.Q. Yu, A. Kudo, Chem. Lett. 34 (2005) 1528.
[13] F. Trifiro, H. Hoser, R.D. Scarle, J. Catal. 25 (1972) 12.
[14] I. Matsuura, R. Schut, K. Hirakawa, J. Catal. 63 (1980) 152.
[15] A.F. Van den Elzen, G.D. Riek, Acta Cryst. B. 29 (1973) 2433.
[16] L.M. Reilly, G. Sanar, C.R.A. Catlow, J. Solid. State. Chem. 148 (1999) 178.
[17] Y. Shimodaira, H. Kato, H. Kobayashi, A. Kudo, J. Phys. Chem. B. 110 (2006) 17790.
[18] A. Kudo, I. Tsuji, H. Kato, Chem. Commun. (2002) 1958.
[19] M.A. Butler, Appl. Phys. 48 (1977) 1914.
[20] G.W. Smith, J.A. Ibers, Acta Crystallogr. 19 (1965) 269.
[21] S.U.M. Khan, J. Akikusa, J. Phys. Chem. B. 103 (1999) 7184.